Capacity Design of Intermediate Horizontal Boundary Elements of Steel Plate Shear Walls

Bing Qu, M.ASCE[1]; and Michel Bruneau, M.ASCE[2]

Abstract: Consistent with capacity design principles and requirements of ductile behavior, the 2005 AISC and 2001 CSA seismic design codes require that the intermediate horizontal boundary elements (HBEs) of steel plate shear walls (SPSWs) be designed to remain essentially elastic with the exception of plastic hinges at their ends when the infill plates fully yield under seismic loading. However, the unexpected failure observed during the tests on a full-scale two-story SPSW suggested that the current design approach does not necessarily lead to an intermediate HBE with the expected performance. This paper presents analytical models for estimating the design forces for intermediate HBEs to reliably achieve capacity design. Those models combine the assumed plastic mechanism with a linear beam model of intermediate HBE considering fully yielded infill panels and are able to prevent in-span plastic hinges. Design forces predicted using the proposed models are compared with those from nonlinear finite element analysis. Good agreement is observed. Finally, the proposed models are also used to explain the observed premature failure of intermediate HBE.

Introduction

A steel plate shear wall (SPSW) consists of unstiffened infill steel panels surrounded by columns, called vertical boundary elements (VBEs), and beams, called horizontal boundary elements (HBEs). These panels are allowed to buckle in shear and subsequently form diagonal tension fields to resist lateral forces. Past experimental studies in the United States, Canada, Japan, Taiwan, and other countries have shown that SPSW can exhibit high initial stiffness, behave in a ductile manner, and dissipate significant amounts of hysteretic energy, which make it a viable option for the design of new buildings as well as for the retrofit of existing constructions [a list of past implementations and literature reviews is available in Sabelli and Bruneau (2007)]. Analytical research on SPSWs has also validated useful models for the design and analysis of this system (Thorburn et al. 1983; Elgaaly et al. 1993; Driver et al. 1997; Berman and Bruneau 2003b). Recent design procedures for SPSWs are provided by the CSA Limit States Design of Steel Structures [Canadian Standards Association (CSA) 2001] and the AISC Seismic Provisions for Structural Steel Buildings [American Institute of Steel Construction (AISC) 2005]. Innovative SPSW designs have also been proposed and experimentally validated to expand the range of applicability of SPSWs (Berman and Bruneau 2003a,b, 2008; Vian and Bruneau 2005).

However, some impediments still exist that may limit the widespread acceptance of this structural system. In particular, there remain uncertainties regarding the seismic behavior of intermediate HBE particularly for those having reduced beam section (RBS) connections. For example, unexpected failures have occurred in the intermediate HBE of a full-scale two-story SPSW experimentally investigated by Qu et al. (2008), which indicates that current design approaches do not necessarily lead to HBEs that meet the requirements of ductile behavior. Note that intermediate HBEs are those having infill panels above and below by opposition to anchor HBEs that have panels only on one side.

Simple models using line elements for boundary frame members (e.g., models conventionally used in SAP2000) are not capable of producing satisfactory results of HBE design forces due to the intrinsic complexity in modeling the strength of plastic hinges in HBE and consequently fail to explain the aforementioned observed premature failure in intermediate HBE of the SPSW. Nonlinear finite element (FE) analysis using three-dimensional shell elements can be used to provide more accurate estimates of design forces for HBEs but is too tedious for broad use for this simple design purpose. Therefore, there is a need to develop a reasonably accurate and more efficient method to estimate the design loads for HBEs.

Such an approach is developed and proposed in this paper. Note that due to space constraints here, this paper focuses on the general case of HBEs with RBS connections. Equivalent procedures for HBEs without RBS connections (i.e., a special case of the general formulation presented here) are presented by Qu and Bruneau (2008). Here, based on the expected plastic mechanism and the principle of superposition, the axial and shear forces in intermediate HBE are determined using free-body diagrams. Ways to avoid in-span plastic hinge in HBE are addressed. Simple free-body diagrams are proposed to determine the moment demands at VBE faces. Following verifications of the above analytical models using nonlinear FE analysis, capacity design procedures taking into consideration the strength of plastic hinges

[1]Assistant Professor, Dept. of Civil and Environmental Engineering, California Polytechnic State Univ., San Luis Obispo, CA 93407 (corresponding author). E-mail: bqu@calpoly.edu

[2]Professor, Dept. of Civil, Structural and Environmental Engineering, Univ. at Buffalo, Buffalo, NY 14260. E-mail: bruneau@buffalo.edu
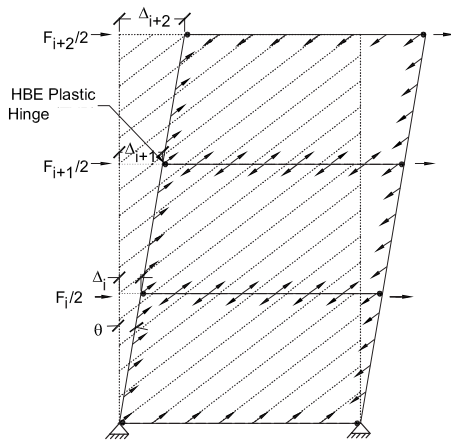
Fig. 1. Expected plastic mechanism of a multistory SPSW

Fig. 2. Decomposition of free-body diagrams of SPSW: (a) typical SPSW; (b) boundary frame with infill panels; (c) boundary frame without infill panels; (d) boundary frame with horizontal components of infill panel yield forces on VBEs; (e) boundary frame with vertical components of infill panel yield forces on HBEs; and (f) boundary frame with horizontal and vertical components of infill panel yield forces on HBEs and VBEs, respectively

subjected to biaxial and shear stress conditions are proposed. Finally, the intermediate HBE of the tested SPSW is examined using the proposed models to explain the unexpected failure observed.

Expected Mechanism and Infill Panel Yield Forces

The desirable plastic mechanism of multistory SPSWs subjected to lateral loads (Berman and Bruneau 2003b) involves uniform yielding of the infill panels over every story (Fig. 1). It provides for possible distributed hysteretic energy over the entire building height (as opposed to a soft-story plastic mechanism in which plastic hinges form in VBEs at a single story). For a multistory SPSW that satisfactorily develops the expected mechanism, the distributed loads applied along the VBEs (ω_{xci} and ω_{yci}) and HBEs (ω_{xbi} and ω_{ybi}) from infill panel yielding at the ith story are

$$\omega_{yci} = R_{yp}f_{yp}t_{wi} \sin 2\alpha/2 \tag{1}$$

$$\omega_{xci} = R_{yp}f_{yp}t_{wi}(\sin \alpha)^2 \tag{2}$$

$$\omega_{ybi} = R_{yp}f_{yp}t_{wi}(\cos \alpha)^2 \tag{3}$$

$$\omega_{xbi} = R_{yp}f_{yp}t_{wi} \sin 2\alpha/2 \tag{4}$$

These are obtained by resolving the infill panel yield forces, occurring at an angle α from the vertical into horizontal and vertical components acting along the VBEs and HBEs. Such components of yield forces per unit lengths are a function of infill panel thickness, t_{wi}, yield strength of infill panels, f_{yp}, and the ratio of expected to nominal yield stress of infill panels, R_{yp} (Berman and Bruneau 2008).

Axial Force in Intermediate HBE

To understand the axial effects in intermediate HBE, consider the multistory SPSW with rigid HBE-to-VBE and VBE-to-foundation connections shown in Fig. 2(a). This SPSW (labeled Frame A) can be decomposed into two lateral force resisting systems for analysis purpose, as shown in Figs. 2(b and c), namely (i) Frame B consisting of infill panels, which resists the lateral loads (i.e., F_{Si} and F_{Si+1}) entirely through infill tension field actions in the boundary frame without moment resisting connections, and (ii)
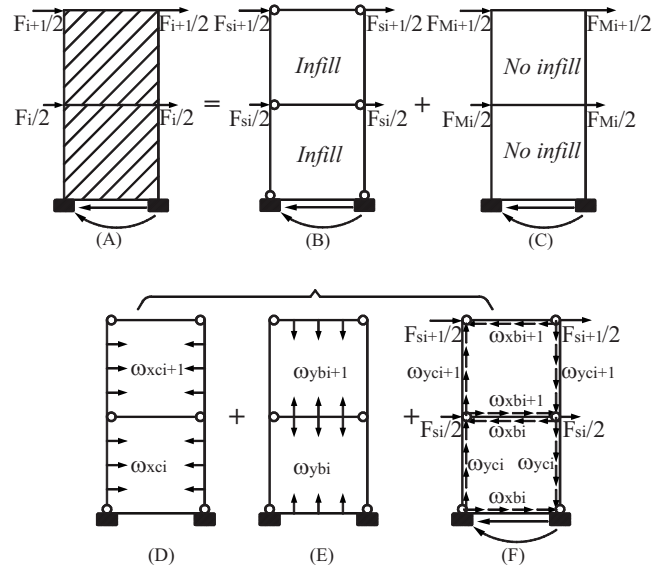
Frame C, which has no infill panels and resists lateral loads (i.e. F_{Mi} and F_{Mi+1}) only through moment frame actions. Note that the HBE end fixities and the VBE base fixities are removed in Frame B since the contribution of those fixities to lateral force resistance is taken into account in Frame C. The summation of lateral force resistances of the above two systems is equal to lateral strength of the SPSW. Incidentally, the strength of the HBE plastic hinges in Frame A must be reduced to account for the presence of significant biaxial and shear stresses in the HBE's web (as discussed later) and determination of the lateral force resistance of Frame C must accordingly consider that effect.

The tension fields applied on Frame B can be further broken into three parts for analysis purpose, namely (i) horizontal components of tension fields applied on VBEs, as shown in Fig. 2(d); (ii) vertical components of tension fields applied on HBEs, as shown in Fig. 2(e); and (iii) horizontal and vertical components of the tension fields applied along HBEs and VBEs, respectively, as shown in Fig. 2(f). Note that Frames D and E are in self-equilibrium and the lateral force resisted by Frame B is applied on Frame F.

Using the principle of superposition, the resulting axial force in the intermediate HBE of Frame A can be obtained by adding up the axial effects in the intermediate HBEs of Frames C, D, E, and F. Note that deformation compatibility is not enforced by this procedure, but this simplifying assumption is expedient (and found to be reasonably accurate) when calculating the axial forces in HBEs. It is recognized that floor slabs in SPSWs could reduce the axial forces in HBEs; however, that effect is conservatively neglected here.

Axial Effects due to Boundary Moment Frame Sway

The behavior of Frame C shown in Fig. 2 is similar to that of a typical steel moment frame. All HBEs are connected to the VBEs
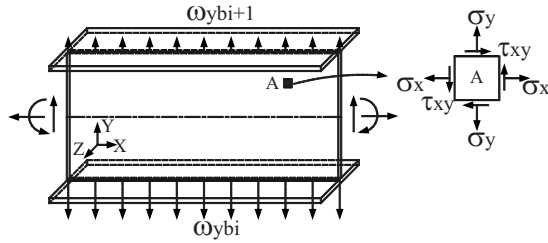
Fig. 3. Intermediate HBE under vertical components of infill panel yield forces

Fig. 4. Assumed HBE axial force distribution due to horizontal components of infill panel yield forces on HBE

using moment resisting connections. For the case shown in Fig. 2(c), where equal equivalent seismic lateral loads are applied on both sides of the frame, no axial forces develop in the HBEs.

Axial Effects of Horizontal Components of Tension Fields on VBEs

To estimate axial forces in the HBEs of Frame D shown in Fig. 2, Berman and Bruneau (2008) proposed a simple analytical model consisting of a continuous beam element representing the VBE supported by elastic springs at the HBE locations. Based on this model, the spring force, P_{Di}, corresponding to compression axial force in HBE, which is typically of significant magnitude, can be estimated from the horizontal components of the tension fields on the VBEs considering VBE lengths tributary to each HBE, i.e.

$$P_{Di} = \omega_{xci}\left(\frac{h_i}{2} - \frac{d}{2}\right) + \omega_{xci+1}\left(\frac{h_{i+1}}{2} - \frac{d}{2}\right) \quad (5)$$

where $h_i = i$th story height and d=depth of the HBE considered.

Axial Effects of Vertical Components of Tension Fields on HBEs

Another (and often neglected) potential source of axial force in HBE is due to deformation compatibility of the HBE web. Axial restraint of a HBE, if present, can lead to axial forces in that HBE when its web is subjected to the vertical components of infill panel yield forces as shown in Fig. 2(e). To illustrate this, consider an element located within the web of an intermediate HBE segment as shown in Fig. 3.

Note that the web of HBE is in plane-stress condition. The axial strain, $\varepsilon_x(y)$, of the considered element can be obtained according to Hooke's law

$$\varepsilon_x(y) = \frac{\sigma_x(y) - \nu\sigma_y(y)}{E} \quad (6)$$

where ν=Poisson's ratio and E=Young's modulus. Stresses $\sigma_x(y)$ and $\sigma_y(y)$ are in-plane-stress components in the coordinate system shown in Fig. 3.

For a HBE with ideally rigid axial restraints, neglecting the restraining effect on HBE web due to the presence of HBE flange, the web of that HBE is unable to elongate along the member's longitudinal axis, which is mathematically expressed as

$$\varepsilon_x(y) = 0 \quad (7)$$

Substituting Eq. (7) into Eq. (6), the relationship between vertical and axial stresses is obtained
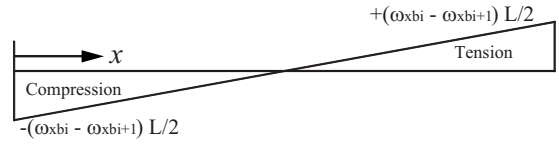
$$\sigma_x(y) = \nu\sigma_y(y) \quad (8)$$

The axial tension due to this Poisson's effect can be obtained by integrating the axial stress along the depth of HBE web

$$P_{Ei} = \int_0^{h_w} \sigma_x(y)t_w dy \quad (9)$$

where t_w and h_w=thickness and depth of HBE web, respectively.

Assuming a linear distribution of vertical stresses in HBE web (Qu and Bruneau 2008)

$$\sigma_y(y) = \frac{\omega_{ybi}}{t_w}\left(1 - \frac{y}{h_w}\right) + \frac{\omega_{ybi+1}}{t_w}\left(\frac{y}{h_w}\right) \quad (10)$$

Substituting Eq. (10) into Eq. (9) and integrating, the axial tension is obtained as

$$P_{Ei} = \frac{\nu(\omega_{ybi} + \omega_{ybi+1})}{2}h_w \quad (11)$$

Although the potential for the above axial force theoretically exists, the magnitude of the contribution of this axial effect to the total axial force in intermediate HBE typically would be on the order of 5% if the VBEs were able to fully restrain the intermediate HBE against axial deformation. Results reported in the available literature have not commented on this effect at the time of this writing, and it is difficult to identify whether this effect has been occurring in prior tests since it is only a small contribution. Furthermore, whether or not HBEs can effectively be restrained axially varies from wall to wall, depending on the fixity at the ends of HBE and the relative stiffness of HBEs and VBEs. It would be interesting in future research to monitor to what extent this effect contributes to structural behavior. However, the FE models presented later include this effect. For consistency, wherever the boundary conditions used in FE studies prevent axial elongation, this effect has to be taken into account to assess the accuracy of proposed simplified approach against such FE benchmark results.

Axial Effects of Horizontal Components of Tension Fields on HBEs

As shown in Fig. 2(f), for which lateral loads are equally applied on both sides of the frame, the axial force resulting from the horizontal components of tension fields acting along HBE varies as shown in Fig. 4. Mathematically, this distribution can be expressed as

$$P_{Fi}(x) = \left(x - \frac{L}{2}\right)(\omega_{xbi} - \omega_{xbi+1}) \quad (12)$$

where L=distance between VBE faces. Note that the above assumption may not be proper when the lateral loads applied on both sides of the SPSW are unequal (Qu and Bruneau 2008).
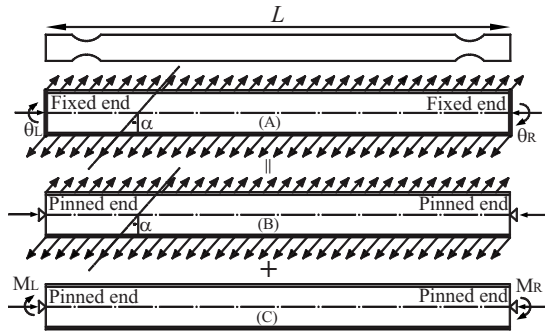
Fig. 5. Decomposition of loading on intermediate HBE: (a) typical intermediate HBE; (b) intermediate HBE subjected to infill panel yield forces; and (c) intermediate HBE subjected to moments at VBE faces

Fig. 6. Decomposition of infill panel yield forces on simply supported beam and shear diagrams

Resulting Axial Force in HBE

The analytical models to estimate axial forces in intermediate HBE have been developed for each subsystem shown in Fig. 2. These axial effects predicted using Eqs. (5), (11), and (12) are then combined, considering an arbitrary sign convention (i.e., "−" and "+" for compression and tension, respectively), resulting in the following equation for the axial force at any location of intermediate HBE:

$$P_{\text{HBE}i}(x) = -\omega_{xci}\left(\frac{h_i}{2} - \frac{d}{2}\right) - \omega_{xci+1}\left(\frac{h_{i+1}}{2} - \frac{d}{2}\right)$$
$$+ \frac{v(\omega_{ybi} + \omega_{ybi+1})h_w}{2} + \left(x - \frac{L}{2}\right)(\omega_{xbi} - \omega_{xbi+1}) \tag{13}$$
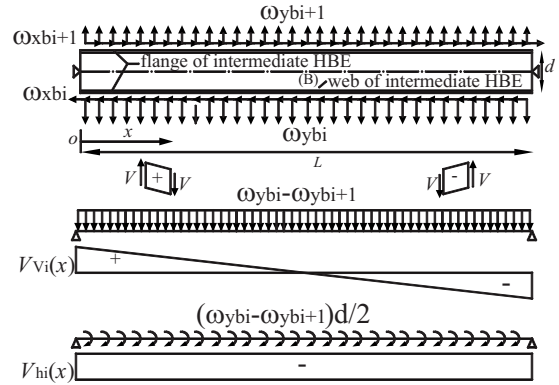
Shear Force in Intermediate HBE

Shear force in an intermediate HBE comes from two sources: tension fields and moment frame sway. To better understand this, decompose the free-body diagram of an intermediate HBE (labeled Beam A in Fig. 5) into two subsystems as shown in Fig. 5, namely (i) Beam B, a simply supported beam subjected to top and bottom tension fields, and (ii) Beam C, also a simply supported beam subjected to moments at VBE faces due to moment frame sway action.

For simplicity, the tension field angle, α, typically close to 45° from the vertical, is assumed to be identical on both sides the HBE. In design, one may alternatively use the average orientation angle of the top and bottom tension fields in the free-body diagram shown in Fig. 5.

Shear Effects Only due to Infill Panel Yield Forces

To obtain the shear effect in HBE due to infill panel yield forces, the tension fields on Beam B shown in Fig. 5 are decomposed into horizontal and vertical components as shown in Fig. 6. To account for the shear effect caused by vertical components of the tension fields (i.e., ω_{ybi+1} and ω_{ybi}), the resulting vertical tension field forces [i.e., $(\omega_{ybi} - \omega_{ybi+1})$] are applied at the HBE centerline as shown in the middle part of Fig. 6. One can obtain the corresponding shear as

$$V_{vi}(x) = \frac{(\omega_{ybi} - \omega_{ybi+1})(L - 2x)}{2} \tag{14}$$

To account for the shear effects generated by the horizontal components of the top and bottom tension fields, a free-body diagram is shown in the bottom part of Fig. 6, in which the horizontal components of the tension fields acting in opposite directions at the top and bottom edges of the HBE web (i.e., ω_{xbi+1} and ω_{xbi}) are equivalently replaced by uniformly distributed moments of magnitude equal to the horizontal components of the tension fields times the distance from the acting line to the beam centerline. One can obtain the corresponding shear as

$$V_{hi}(x) = -\frac{(\omega_{xbi} + \omega_{xbi+1})d}{2} \tag{15}$$

By combining the shear force predicted in Eqs. (14) and (15), one can obtain the shear forces in an intermediate HBE due to the top and bottom tension fields

$$V_{Bi}(x) = \frac{(\omega_{ybi} - \omega_{ybi+1})(L - 2x)}{2} - \frac{(\omega_{xbi} + \omega_{xbi+1})d}{2} \tag{16}$$

Prior to this study, the shear force in HBE due to infill panel yield forces was estimated using simple line models, in which HBE depth was usually neglected. Correspondingly, the design shear force at each end of HBE was determined using Eq. (14).

To compare the adequacy of the analytical model proposed in this paper for estimating the shear forces in intermediate HBE due to infill panel yield forces with that used in prior design, two different examples were investigated using FE method. Those two examples consider intermediate HBEs under either equal or unequal top and bottom tension fields.

The HBEs modeled consisted of a 3,508-mm-long W24×76 beam. An orientation angle of $\alpha=45°$ was assumed for the top and bottom tension fields in all cases. Material was assumed to be A572 Grade 50 steel with isotropic and elastoperfectly plastic constitutive behavior. The considered magnitudes of top and bottom tension fields are summarized in Table 1.

The FE models were analyzed in ABAQUS/Standard using shell element (ABAQUS element S4R). A total number of 17,280 elements were used for the HBE. The ends of the beams were simply supported. The top and bottom tension field forces were applied on the FE models. The shear forces at the VBE faces obtained from FE analyses are presented in Table 1, together with the shear forces predicted using the proposed model and those from the previously used model.

Table 1. Shear Forces at VBE Faces due to Infill Panel Yield Forces

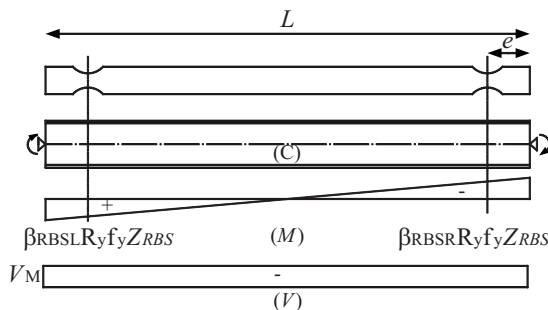| HBE	ω_{xbi} (N/mm)	ω_{ybi} (N/mm)	ω_{xbi+1} (N/mm)	ω_{ybi+1} (N/mm)	Left VBE face shear (kN)			Right VBE face shear (kN)		
					FE	Eq. (16)	Eq. (14)	FE	Eq. (16)	Eq. (14)
1	496	496	496	496	292.5	292.5	0	−292.5	−292.5	0
2	496	496	357	357	6.7	6.7	244.7	−496.1	−496.1	−244.7

As compared in Table 1, the estimates of HBE end shears using the proposed model agree well with the FE results. However, the previously used model fails to capture the important variation of shear forces at the ends of intermediate HBE that occurs because the resultant action of the vertical tension field components is not equally resisted by each end of the HBE.

Shear Effects due to Moment Frame Sway Action Alone

Shear effects in HBE due to frame sway action alone (i.e., shear in Beam C shown in Fig. 5) is straightforward and a well known result. The free-body diagram, moment diagram, and shear diagram are shown in Fig. 7. Parameter e represents the distance from plastic hinge to VBE face.

The flexural strength of HBE plastic hinges (assumed to be at the center of the RBS) must be reduced to account for the presence of significant biaxial and shear stresses in their web (note that, contrary to beams in moment frames, the HBEs of SPSWs can be under considerable vertical axial stresses). An analytical procedure was proposed by Qu and Bruneau (2008) to quantify the non-negligible impact of these stresses by using the von Mises yield criterion to reduce the web's axial yield strength as a function of the combined shear and vertical stresses acting in the HBE web. Solutions for the reduced plastic moment of intermediate HBE under equal top and bottom tension fields were first derived and extended to intermediate HBEs under unequal top and bottom tension fields by assuming a linear distribution of vertical stresses in the HBE web. Both positive and negative flexure cases were considered and found to be differently affected by the biaxial stress field (where positive or negative flexure refers to the bending action producing tension or compression in the HBE flange, respectively, on which the greater magnitude of the tension field is applied). The proposed procedure and simplified analytical models were validated by FE analysis.

Here, to illustrate the effects of biaxial and shear stresses in HBE web on HBE plastic moment, a typical result for the simpler case of intermediate HBE under equal top and bottom tension fields is presented in Fig.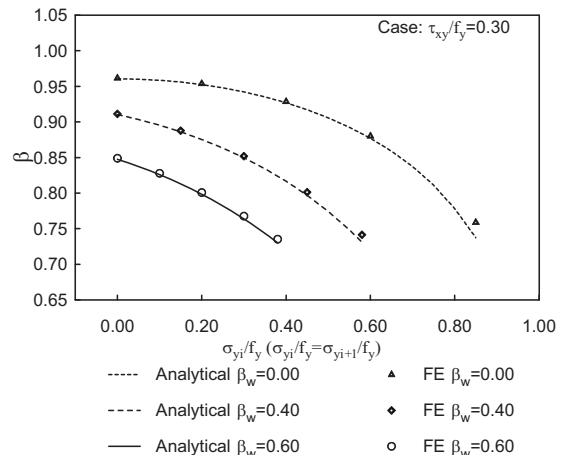 8. In the figure, β (defined as the cross section plastic moment reduction factor) is the ratio of available to nominal plastic flexural strength of HBE; τ_{xy} is the shear stress in the HBE web, σ_{yi+1} and σ_{yi} are the vertical stresses at the top and bottom edges of the intermediate HBE web, respectively; and β_w is the ratio of applied axial compression to the nominal axial strength of HBE web. As shown, the cross section plastic moment reduction factor, β, reduces as a result of increasing axial force, shear stress, and vertical stresses. For example, for the load combination, $\beta_w=0.40$ and $\tau_{xy}/f_y=0.30$, β has a value of 0.91 when no vertical stress exists in the HBE web (i.e., when $\sigma_{yi}/f_y=\sigma_{yi+1}/f_y=0$, which corresponds to a member in a conventional steel moment frame); however, β reduces to a smaller value of 0.73 when $\sigma_{yi}/f_y=\sigma_{yi+1}/f_y=0.58$. Incidentally, for an intermediate HBE under unequal top and bottom tension fields, closed-form solutions are too complex for design practice and a simplified approach that gives reasonably accurate results has been proposed and validated [see Qu and Bruneau (2008) for details of that procedure].
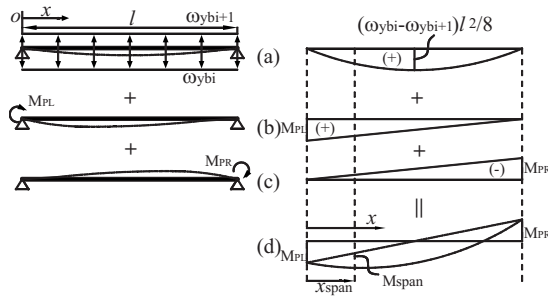
Taking into account the cross section plastic moment reduction factors derived per the above procedure and neglecting strain hardening, the uniform shear in HBE only due to moment frame sway action can be expressed as

$$V_M = -\frac{(\beta_{RBSL} + \beta_{RBSR})R_y f_y Z_{RBS}}{L - 2e} \qquad (17)$$

where Z_{RBS}=plastic section modulus of the assumed plastic hinge; f_y=HBE yield strength; β_{RBSL} and β_{RBSR}=cross section plastic moment reduction factors of left and right HBE plastic hinges that can be obtained using the procedure briefly summarized above; and R_y=ratio of expected to nominal yield stress of steel. Note that iterations may be necessary in design since the plastic moment reduction factors, β_{RBSL} and β_{RBSR}, depend on the total shear forces acting at the plastic hinges and that these must be assumed at the beginning of the design process.

Fig. 7. Free body diagram, moment diagram, and shear diagram of HBE with RBS connections under plastic end moments due to moment frame sway

Fig. 8. Typical result comparisons

Fig. 9. Deformed shape, loading, and moment diagrams of intermediate HBE: (a) vertical components of infill panel forces; (b) left-end redundant moment; (c) right-end redundant moment; and (d) combined moment diagram

Resulting Shear Force in HBE

Combining the shear effects predicted using Eqs. (16) and (17) (i.e., shear effects due to infill panel yield forces and moment frame sway, respectively), the resulting shear force in HBE is

$$V_{\text{HBE}i}(x) = \frac{(\omega_{ybi} - \omega_{ybi+1})(L - 2x)}{2} - \frac{(\omega_{xbi} + \omega_{xbi+1})d}{2}$$
$$- \frac{(\beta_{\text{RBS}L} + \beta_{\text{RBS}R})R_y f_y Z_{\text{RBS}}}{L - 2e} \quad (18)$$

Prevention of In-Span HBE Plastic Hinge

According to the design codes (AISC 2005; CSA 2001), with the exception of plastic hinges at their ends, HBEs must be designed to remain essentially elastic when the plastic mechanism of the wall develops. An in-span plastic hinge is deemed to be undesirable because of the corresponding amplified beam deflections that would develop at that location, which could prevent a uniform distribution of yielding across the infill panels. Vian and Bruneau (2005) proposed a procedure to prevent in-span plastic hinges in anchor HBE. Here, the moment diagram used in their procedure is applied to intermediate HBE by considering the resulting distributed forces from top and bottom tension fields. That procedure is extended to account for the reduced plastic moment of HBE due to the presence of axial compression, shear force, and vertical stresses.

Vian and Bruneau (2005) obtained the moment diagram for an anchor HBE by superposing plastic HBE end moments due to moment frame sway and a quadratic "hanging" moment due to the vertical components of the infill panel yield forces. Following this logic, the moment diagram of an intermediate HBE can be obtained as shown in Fig. 9.

Using the sign convention shown in Fig. 9, equation for the resulting moment diagram is

$$M(x) = \frac{(\omega_{ybi} - \omega_{ybi+1})x}{2}(l - x) - M_{PR}\frac{x}{l} + M_{PL}\left(1 - \frac{x}{l}\right) \quad (19)$$

where M_{PL} and M_{PR}=plastic moments at the left and right ends of the beam, respectively, and l=distance between left and right plastic hinges. For a HBE with RBS connection, l can be taken as $L-2e$, where L is the distance between VBE faces as previously defined.

The location of the maximum moment, x_{span}, is calculated by differentiating $M(x)$ with respect to x, setting the result equal to zero, and solving

$$x_{\text{span}} = \frac{l}{2} - \left[\frac{M_{PL} + M_{PR}}{(\omega_{ybi} - \omega_{ybi+1})l}\right] \quad (20)$$

Theoretically, x_{span} can be anywhere from negative infinity to $l/2$. However, the location of maximum moment will be out of the span if x_{span} is less than zero, which implies that plastic hinges can only form at HBE ends.

Substituting into Eq. (20) into Eq. (19) and simplifying, one can obtain the maximum moment as

$$M_{\text{span}} = \frac{(\omega_{ybi} - \omega_{ybi+1})l^2}{8} + \frac{(M_{PL} + M_{PR})^2}{2(\omega_{ybi} - \omega_{ybi+1})l^2} + \frac{M_{PL} - M_{PR}}{2} \quad (21)$$

To prevent in-span HBE plastic hinge, the maximum in-span flexural demand should be smaller than the available plastic strength

$$M_{\text{span}} \leq \beta_S R_y f_y Z \quad (22)$$

where β_S=plastic moment reduction factor at the location of maximum moment. Similar to $\beta_{\text{RBS}L}$ and $\beta_{\text{RBS}R}$, β_S can be determined following the procedure proposed by Qu and Bruneau (2008).

The plastic moments at the left and right ends can be obtained as

$$M_{PL} = \beta_{\text{RBS}L}\eta R_y f_y Z \quad (23)$$

$$M_{PR} = \beta_{\text{RBS}R}\eta R_y f_y Z \quad (24)$$

respectively, where η referred to here as the RBS *plastic section modulus reduction ratio* can be obtained as

$$\eta = \frac{Z_{\text{RBS}}}{Z} \quad (25)$$

Substituting Eqs. (23) and (24) into Eq. (21), replacing l in Eq. (21) by $L-2e$, and considering the constraint expressed in Eq. (22), one can obtain the lower bound of plastic section modulus of intermediate HBE

$$Z_{\text{min}} = \frac{(\omega_{ybi} - \omega_{ybi+1})(L - 2e)^2}{4R_y f_y} \frac{1}{\beta_{1R} + \sqrt{\beta_{1R}^2 - \beta_{2R}^2}} \quad (26)$$

where

$$\beta_{1R} = \beta_S + \frac{(\beta_{\text{RBS}R} - \beta_{\text{RBS}L})\eta}{2} \quad (27)$$

$$\beta_{2R} = \frac{(\beta_{\text{RBS}R} + \beta_{\text{RBS}L})\eta}{2} \quad (28)$$

Moment Demands at VBE Faces

For intermediate HBE having RBS connections, it is necessary to check the adequacy of flexural strength at VBE face to ensure the satisfactory behavior of HBE. Assuming plastic hinges develop at RBS centers, simple free-body diagrams are developed in Fig. 10 for determining the moment demand at VBE face. In Fig. 10 P_R and P_L represent axial forces at the right and left VBE faces; M_R and M_L represent moment demands at the right and left VBE
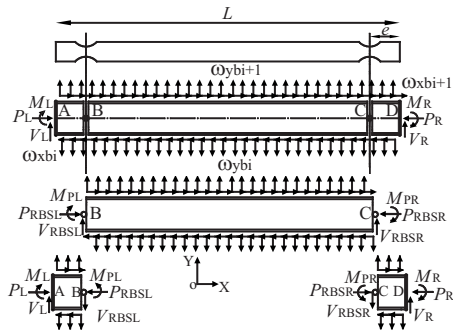
Fig. 10. Free body diagrams of intermediate HBE for calculation of moment demand at VBE face

faces; V_R and V_L represent shear forces at the right and left VBE faces; P_{RBSR} and P_{RBSL} represent axial forces at the right and left plastic hinges; V_{RBSR} and V_{RBSL} represent shear forces at the right and left plastic hinges; and M_{PR} and M_{PL} represent the reduced plastic moments at the right and left plastic hinges that can be determined using Eqs. (23) and (24), respectively. For analysis purpose, the beam is divided into three segments, the middle segment between two plastic hinges and the right and left segments outside of the plastic hinges.

For middle portion of the beam (i.e., Segment BC shown in Fig. 10), solving for V_{RBSR} from the moment equilibrium to the left plastic hinge (i.e., Point B) gives

$$V_{\text{RBS}R} = \frac{(M_{PR} + M_{PL})}{L - 2e} + \frac{(\omega_{ybi} - \omega_{ybi+1})(L - 2e)}{2} + \frac{(\omega_{xbi} + \omega_{xbi+1})d}{2}$$

(29)

Similarly, using the moment equilibrium to the right plastic hinge (i.e., Point C), one can obtain

$$V_{\text{RBS}L} = \frac{(\omega_{ybi} - \omega_{ybi+1})(L - 2e)}{2} - \frac{M_{PR} + M_{PL}}{L - 2e} - \frac{(\omega_{xbi} + \omega_{xbi+1})d}{2}$$

(30)

For right segment of the HBE (i.e., beam segment CD shown in Fig. 10), solving for M_R from the moment equilibrium to the right VBE face (i.e., point D) gives

$$M_R = M_{PR} + V_{\text{RBS}R}e + \frac{(\omega_{ybi} - \omega_{ybi+1})e^2}{2} - \frac{(\omega_{xbi} + \omega_{xbi+1})de}{2}$$

(31)

Similarly, for left segment of the HBE (i.e., beam Segment AB shown in Fig. 10), the moment equilibrium to the left VBE face (i.e., Point A) gives

$$M_L = M_{PL} - V_{\text{RBS}L}e - \frac{(\omega_{ybi} - \omega_{ybi+1})e^2}{2} - \frac{(\omega_{xbi} + \omega_{xbi+1})de}{2}$$

(32)

Note that the moment demands at VBE faces determined from Eqs. (31) and (32) should compare with the available flexural strengths at the right and left VBE faces, $M_{R.\text{Strength}}$ and $M_{L.\text{Strength}}$, respectively,

$$M_{R.\text{Strength}} = \beta_R R_y f_y Z$$

(33)

$$M_{L.\text{Strength}} = \beta_L R_y f_y Z$$

(34)

where β_R and β_L = cross section plastic moment reduction factors of the right and left VBE faces and can be determined using the procedure proposed by Qu and Bruneau (2008).

FE Verification and Design Recommendation

To check the adequacy of the analytical models proposed in this paper to determine the HBE design forces and to prevent the in-span HBE plastic hinge, FE analyses were conducted. Using the specimen described in Qu et al. (2008) as a prototype SPSW, the intermediate HBE was redesigned using the design forces predicted from the analytical models developed in previous sections. The resulting new intermediate HBE is a W24×76 member. RBS connections were also used in the new HBE. The cross section properties and flange reduction geometries of the redesigned and original members are summarized in Table 2.

The redesigned intermediate HBE was modeled in ABAQUS/Standard using shell elements (ABAQUS element, S4R). A total of 17,280 elements were used in the model. Material was assumed to have a yield strength of 346 MPa with isotropic and elastoperfectly plastic behavior.

The FE analysis was conducted in two stages. In the first stage, the uniformly distributed loads, ω_{yb1}, ω_{xb1}, ω_{yb2}, and ω_{xb2}, which were determined to be 557, 492, 400, and 353 N/mm, respectively, using the actual thicknesses, yield strengths, and inclination angles of the infill panels at the first and second story of specimen, were applied along the top and bottom edges of the HBE web to represent the infill panel yield forces. At the same time, both ends of the beam were fully fixed except that the axial restraint at the right end was released and an axial load that was determined by setting $x=L$ in Eq. (13) was applied to replicate the axial force in the HBE. In the second stage, a displacement controlled method was used. HBE end rotations with identical magnitude up to 0.035 rad, which corresponded to rightward sway of the SPSW, were applied at the ends of the HBE to obtain the shear and moment demands at VBE faces. Note that design forces at the right VBE face governed the design.

In the FE model, no in-span plastic hinge was observed in the redesigned HBE. The axial forces, shear forces, and moment demands at the left and right VBE faces obtained from the FE analy-

Table 2. Cross-Sectional Properties and Flange Reduction Geometries

HBE	d (mm)	b_f (mm)	t_f (mm)	t_w (mm)	a[a] (mm)	b[a] (mm)	c[a] (mm)	Z (mm^3)	Z_{RBS} (mm^3)
Original	350	252	19	11	135	230	48	1.85×10^6	1.25×10^6
Redesigned	607	228	17.3	11.2	160	486	57	3.27×10^6	2.08×10^6

[a]Flange reduction geometry parameters described in Fig. 16.

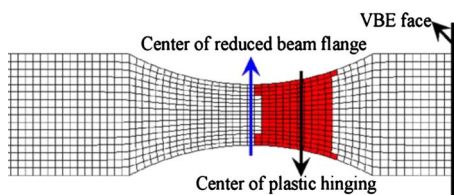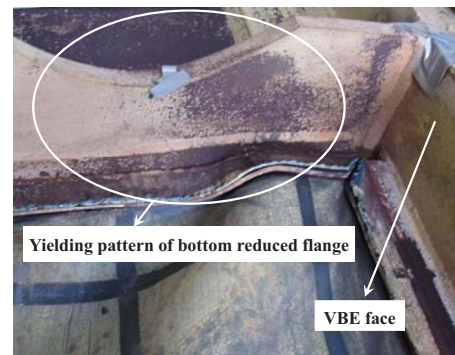**Table 3.** Design Forces at VBE Faces

| VBE face	Design forces	Finite-element analysis	Plastic analysis based on free-body diagrams with plastic hinge location taken as			
			Center of RBS		Proposed for design	
			Value	Error (%)	Value	Error (%)
Left	Axial force (kN)	1,426	1,426	[a]	1,426	[a]
	Shear force (kN)	432	395	−8.6	455	5.3
	Moment (kN m)	729	632	−13	809	11
Right[b]	Axial force (kN)	941	941	[a]	941	[a]
	Shear force (kN)	981	945	−3.7	1,005	2.4
	Moment (kN m)	875	842	−3.8	876	0.1

[a]Not applicable.

[b]Control the design.

sis are presented in Table 3, together with those predicted using the proposed analytical models. As shown, the predictions agree reasonably well with the FE results. The difference between the predictions and FE results mainly comes from the simplification of plastic hinge location in the free-body diagrams shown in Figs. 8 and 10, in which the plastic hinges are assumed to form ideally at the center of the RBS. However, it is not the actual case due to the presence of variable axial force, shear force, and vertical stresses in HBE.

To illustrate the actual location of plastic hinging in a HBE, the yielding pattern of the bottom flange at the right RBS connection at the onset of inelastic behavior obtained from the FE analysis is shown in Fig. 11. The yielding zones are represented by the shaded areas. This shows that the center of the yielding zone (and thus the location of the lumped plastic hinge) moves toward the near VBE face. At the time of this writing, no experiments have been conducted on the redesigned HBE to confirm the above observations from FE analysis. However, similar yielding patterns were consistently observed during the tests of Qu et al. (2008) as shown in Fig. 12 and tests recently conducted at NCREE as shown in Fig. 13. Note that the yielding parts in the specimens are represented by the flaked whitewash. The yielding pattern in the web of the redesigned HBE at the end of the FE analysis is presented in Fig. 14. As shown, the yielding zones spread over a large area in the HBE web due to the presence of significant biaxial and shear stresses. Similar yielding behavior was also consistently observed during the tests of Qu et al. (2008) as shown in Fig. 15.

In design, for greater accuracy, it is possible to account for the actual location of plastic hinge. Calculation of the distance from the center of the reduced beam flange to the actual plastic hinge location toward the VBE face can be simplified by assuming that the plastic section modulus of the actual plastic hinge is equal to the average of the plastic section moduli of the unreduced part of

Fig. 12. Flange of the intermediate HBE of SPSW (at the early stage of testing) (Qu et al. 2008)

(a)

(b)
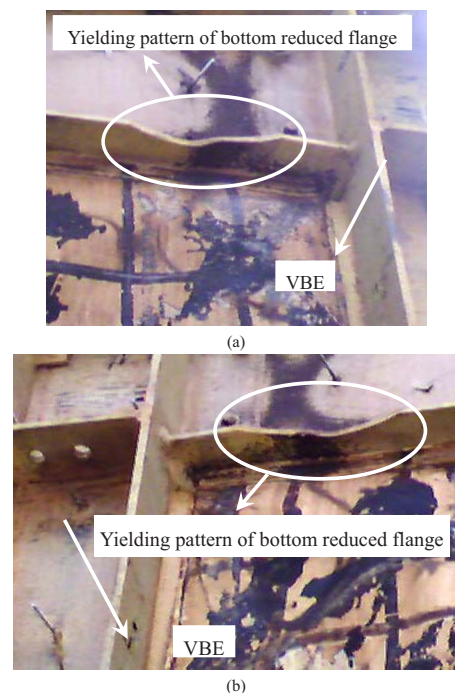
Fig. 13. Flange of the intermediate HBE in recent testing (K. C. Tsai and NCREE, personal communication, 2007, photo by M. Bruneau)

Fig. 11. Flange of the redesigned intermediate HBE-FE model (at the onset of inelastic behavior)
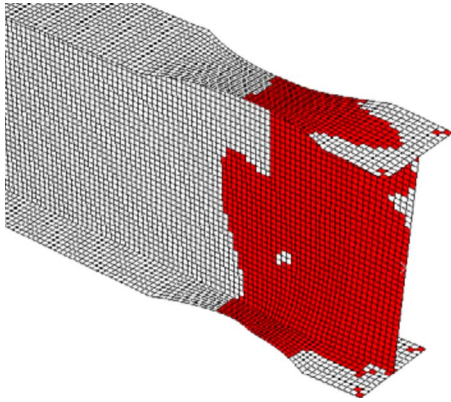
Fig. 14. Web of the redesigned intermediate HBE-FE model (at the end of the FE analysis)

the HBE and that at the RBS center. Accordingly, the plastic section modulus of the plastic hinge is modified as

$$Z_{RBS} = \frac{(1 + \eta)}{2} Z \qquad (35)$$

The distance, e, as shown in Figs. 7 and 10, is determined as

$$e = a + \frac{b}{2} - \Delta x \qquad (36)$$

where Δx=distance between RBS center and the assumed plastic hinge shown in Fig. 16

$$\Delta x = \sqrt{2 \Delta y R - \Delta y^2} \qquad (37)$$

$$\Delta y = \frac{(1 - \eta)Z}{4 t_f (d - t_f)} \qquad (38)$$

$$R = \frac{4c^2 + b^2}{8c} \qquad (39)$$

Beyond this difference, the rest of the procedure established on the basis of free-body diagrams shown in Figs. 7 and 10 remain valid. Results obtained using this modified approach are presented in Table 3. It is observed that this modified approach provides more accurate estimate for moment at the side governing the design (i.e., right VBE face). For shear, the accuracy is not significantly improved, however, at least, the modified approach

Fig. 15. Web of the intermediate HBE of SPSW at the end of testing (Qu et al. 2008)
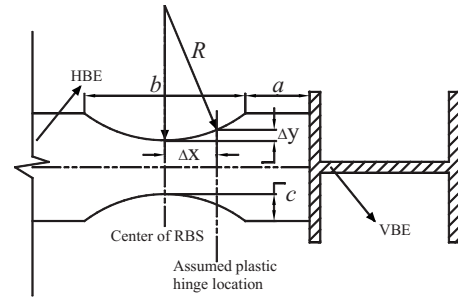
**Fig. 16.** Modification of plastic hinge location

provides conservative estimate by 2.4% as supposed to be unconservative by 3.7% from the model assuming plastic hinge developed at the center of RBS.

Capacity Design Procedures

Based on the analytical modes developed in this paper, capacity design procedures are proposed for intermediate HBEs having RBS connections in SPSWs. It differs from the current design approach in that it (i) considers reduced plastic moment strength of HBE to account for the presence of axial load, shear force, and vertical stresses in HBE; (ii) is able to capture the fact that resultant action of the vertical tension field components is not equally resisted by each end of HBE; and (iii) accounts for the variation of plastic hinge location in HBE.

The procedure for capacity design of an intermediate HBE having RBS connections is illustrated in Fig. 17. Design steps of this procedure are outlined below

Step 1: Calculate the infill panel yield forces per Eqs. (1)–(4).

Step 2: Assume an intermediate HBE cross section.

Step 3: Determine the axial force in HBE per Eq. (13).

Step 4: Determine the vertical stresses in HBE web using the procedure proposed by Qu and Bruneau (2008).

Step 5: Select the flange reduction geometries in compliance with the design specifications and guidelines such as FEMA 350 [Federal Emergency Management Agency (FEMA) 2000].

Step 6: In accordance with Fig. 16, determine the plastic section modulus and location of plastic hinge per Eqs. (35) and (36).

Step 7: Assume plastic moment reduction factors of the plastic hinges (β_{RBSR} and β_{RBSL}) for the initial iteration of the design process.

Step 8: Determine the shear forces at plastic hinges per Eq. (18).

Step 9: Based on the approaches proposed by Qu and Bruneau (2008), calculate the plastic moment reduction factors at plastic hinges. If the calculated factors are close enough to those assumed in Step 7, continue the design. Otherwise, return to Step 7 and modify the assumed plastic moment reduction factors.

Step 10: Calculate the maximum moment location in HBE per Eq. (20). If the obtained result is negative, which means the maximum moment develops out of span, go to Step 11. Otherwise, calculate the plastic moment reduction factor at the maximum moment location and check Eq. (26). If Eq. (26) is satisfied, continue the design. Otherwise, return to Step 2 and modify the assumed HBE cross section.

Step 11: Calculate the shear forces at VBE faces per Eq. (18).

Step 12: Determine the plastic moment reduction factors at VBE faces (i.e., β_R and β_L).

JOURNAL OF STRUCTURAL ENGINEERING © ASCE / JUNE 2010 / **673**
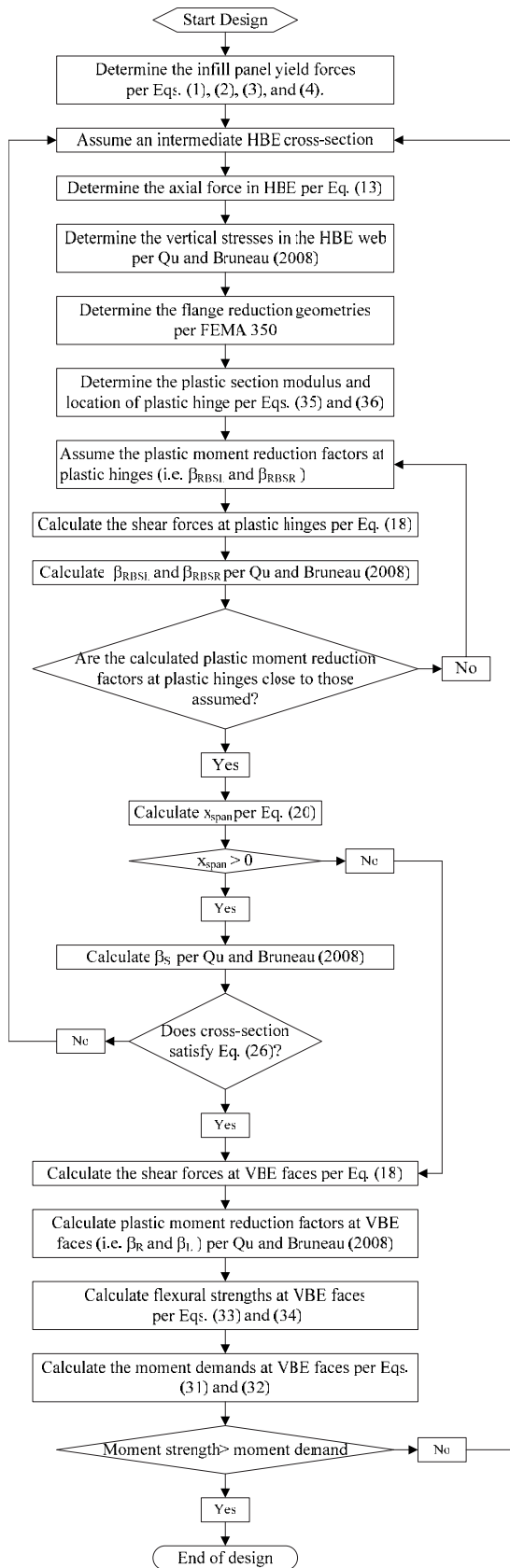
Fig. 17. Design flowchart for intermediate HBE having RBS connections

Table 4. Design Demands and Available Strengths at VBE Faces

HBE	Left VBE face		Right VBE face	
	$M_{L.\text{Demand}}$ (kN m)	$M_{L.\text{Strength}}$ (kN m)	$M_{R.\text{Demand}}$ (kN m)	$M_{R.\text{Strength}}$ (kN m)
Original	660	774	748	571
Redesigned	809	951	876	897

Step 13: Calculate the flexural strengths at VBE faces per Eqs. (33) and (34).

Step 14: Calculate the moment demands at VBE faces per Eqs. (31) and (32).

Step 15: Compare the strengths and demands obtained from Steps 13 and 14, respectively. If the strengths are greater than the demands, complete the design. Otherwise, return to Step 2 and modify the assumed HBE cross section.

It should be noted that gravity loads have not been considered in the free-body diagrams, as they will usually be relatively small in SPSWs. However if so desired, they can be considered by adding them to the vertical components of the infill panel yield forces that are applied to the intermediate HBE. Additionally, derivations in this paper neglect strain hardening since steel in the verification FE example was assumed to have an elastoperfectly plastic constitutive behavior. However, to achieve capacity design, the factor, C_{pr}, to account for strain hardening as per FEMA 350 (FEMA 2000) should be incorporated into determination of the plastic hinge strength in RBS. Another consideration that has not been included is the effect of fish plate along HBE that is used to connect the infill panels; however, that effect was shown to be negligible (Qu and Bruneau 2008). Furthermore, anchor HBEs, as a special case of intermediate HBEs, may be also considered by the proposed procedure with a tension field acting on only one side.

Examination of Intermediate HBE Fractures in Tests

As described in Qu et al. (2008), during testing of a two-story SPSW, the intermediate HBE, which used RBS connections, developed complete fractures at the ends of its bottom flange, but no fractures developed in the reduced beam flange regions. Although many effects may have contributed to this unexpected failure of intermediate HBE, flexural strength deficiency at VBE face is a factor worthy of investigation.

A preliminary assessment can be made by comparing the design moment demands and available flexural strengths at the VBE faces. Based on the intermediate HBE design procedure illustrated in Fig. 17, the flexural demands and strengths of the original HBE were obtained and presented in Table 4.

The effects of material strain hardening, composite floor, and ancillary floor truss [which were used to transfer the load from the actuators to the specimen during the tests, as described by Qu et al. (2008)] are neglected here for simplicity. Note that these effects result in higher plastic hinge moments and higher design demands at VBE faces. For comparison purpose, the design moments and strengths of the redesigned intermediate HBE are also provided in Table 4. The redesigned HBE is a W24×76 member, as described earlier.

As shown in Table 4, at the right VBE face, the flexural strength of the original HBE is smaller than the demand. This would explain the unexpected failure (i.e., fractures at the HBE ends) observed during the tests. By comparison, although higher

demands exist, strengths of the redesigned HBE are greater than demands, suggesting it would not have likely suffered from the observed premature failure.

Conclusions

This paper presented analytical models to estimate design forces for intermediate HBE having RBS connections based on the plastic mechanisms and simple free-body diagrams. A design procedure to achieve capacity design has been proposed. This procedure prevents in-span HBE plastic hinge and ensures moment adequacy at VBE faces. FE analyses were used to validate the proposed approach. Using the knowledge and methodologies developed in this paper, behavior of the intermediate HBE in a tested SPSW was examined, and the observed yielding patterns and premature fractures were explained.

Acknowledgments

References

American Institute of Steel Construction (AISC). (2005). *Seismic Provisions for Structural Steel Buildings*, American Institute of Steel Construction, Chicago.

Berman, J. W., and Bruneau, M. (2003a). "Experimental investigation of light-gauge steel plate shear walls for the seismic retrofit of buildings." *Technical Rep. No. MCEER-03-0001*, Multidisciplinary Center for Earthquake Engineering Research, Buffalo, New York.

Berman, J. W., and Bruneau, M. (2003b). "Plastic analysis and design of steel plate shear walls." *J. Struct. Eng.*, 129(11), 1448–1456.

Berman, J. W., and Bruneau, M. (2008). "Capacity design of vertical boundary elements in steel plate shear walls." *Eng. J.* 45(1), 57–71.

Canadian Standards Association (CSA). (2001). "Limit states design of steel structures." *CAN/CSA S16-01*, Willowdale, Ont.

Driver, R. G., Kulak, G. L., Kennedy, D. J. L., and Elwi, A. E. (1997). "Seismic behavior of steel plate shear walls." *Structural Engineering Rep. No. 215*, Univ. of Alberta, Edmonton, Alta.

Elgaaly, M., Caccese, V., and Du, C. (1993). "Postbuckling behavior of steel-plate shear walls under cyclic loads." *J. Struct. Eng.*, 119(2), 588–605.

Federal Emergency Management Agency (FEMA). (2000). "Recommended seismic design criteria for new steel moment-frame buildings." *FEMA 350*, SAC Joint Venture for FEMA, Washington, D.C.

Qu, B., and Bruneau, M. (2008). "Seismic behavior and design of boundary frame members of steel plate shear walls." *Technical Rep. No. MCEER-08-0012*, Multidisciplinary Center for Earthquake Engineering Research, Buffalo, New York.

Qu, B., Bruneau, M., Lin, C. H., and Tsai, K. C. (2008). "Testing of full scale two-story steel plate shear walls with RBS connections and composite floor." *J. Struct. Eng.*, 134(3), 364–373.

Sabelli, R., and Bruneau, M. (2007). *Steel plate shear walls (AISC design guide)*, American Institute of Steel Construction, Chicago.

Thorburn, L. J., Kulak, G. L., and Montgomery, C. J. (1983). "Analysis of steel plate shear walls." *Structural Engineering Rep. No. 107*, Dept. of Civil Engineering, Univ. of Alberta, Edmonton, Alta.

Vian, D., and Bruneau, M. (2005). "Steel plate shear walls for seismic design and retrofit of building structure." *Technical Rep. No. MCEER-05-0010*, Multidisciplinary Center for Earthquake Engineering Research, Buffalo, New York.